

High Order Hierarchical Asymptotic Preserving Nodal Discontinuous Galerkin IMEX Schemes For The BGK Equation ¹

Tao Xiong ² and Jing-Mei Qiu³

Abstract A class of high order asymptotic preserving (AP) schemes has been developed for the BGK equation in Xiong et. al. (2015) [37], which is based on the micro-macro formulation of the equation. The nodal discontinuous Galerkin (NDG) method with Lagrangian basis functions for spatial discretization and globally stiffly accurate implicit-explicit (IMEX) Runge-Kutta (RK) scheme as time discretization are introduced with asymptotic preserving properties. However, it is only necessary to solve the kinetic equation when the hydrodynamic description breaks down. Motivated by the recent work in Filbet and Rey (2015) [23], it is more naturally to construct a hierarchy scheme under the NDG-IMEX framework without hybridization, as the formal analysis in [37] shows that when ε is small, the NDG-IMEX scheme becomes a local discontinuous Galerkin (LDG) scheme for the compressible Navier-Stokes equations, and when $\varepsilon = 0$ it is a discontinuous Galerkin (DG) scheme for the compressible Euler equations. Moreover, we propose to combine the kinetic regime with the hydrodynamic regime including both the compressible Euler and Navier-Stokes equations. Numerical experiments demonstrate very decent performance of the new approach. In our numerics, all three regimes are clearly divided, leading to great savings in terms of the computational cost.

Keywords: Hierarchy scheme, Compressible Euler Equations, Compressible Navier-Stokes Equations, Asymptotic Preserving, Nodal Discontinuous Galerkin, IMEX, BGK equation

1 Introduction

In physics, rarefied gases can be modeled by kinetic description using the Boltzmann equation. In such a description, Knudsen number ε is an important dimensionless parameter, defined as the ratio of the molecular mean free path length to a representative physical length scale, characterizing the frequency of molecular collisions or how rarefied the gas is. In the zero limit of Knudsen number, the compressible Euler system describing the conservation of mass, moment and energy is a sufficient macroscopic model, while when the Knudsen is sufficiently small but not zero, the compressible Navier-Stokes equations including a correction term on viscosity and heat conductivity are needed. BGK equation is a simplified model for the Boltzmann equation, which is introduced by Bhatnagar, Gross and Krook [9], in a hyperbolic scaling.

Many numerical schemes have been proposed for solving the BGK and Boltzmann equations with a wide range of Knudsen number. A micro-macro decomposition framework was proposed by Bennoune, Lemou, Mieussen [8], which can correctly capture the macroscopic

¹Research supported by NSF DMS-1217008, DMS-1522777 and Air Force Office of Scientific Computing FA9550-12-0318 and the Fundamental Research Funds for the Central Universities No. 20720160009.

²School of Mathematical Sciences, Fujian Provincial Key Laboratory of Mathematical Modeling and High-Performance Scientific Computing, Xiamen University, Xiamen, Fujian, P.R. China, 361005. Email: txiong@xmu.edu.cn

³Department of Mathematics, University of Houston, Houston, 77004. E-mail: jingqiu@math.uh.edu.

Navier-Stokes limit when the Knudsen number is sufficiently small. Various versions of implicit-explicit schemes were proposed for the BGK equations in [31, 32] and for the ES-BGK equation in [22]. A BGK-penalization strategy was proposed by Filbet and Jin [21] for the Boltzmann equation. These methods are all related to the asymptotic preserving (AP) schemes, which are designed to mimic the asymptotic limit from the kinetic to the hydrodynamic models on the PDE level as ε goes to 0 [25].

A family of high order AP schemes for the BGK equation has been developed in [37], based on the micro-macro decomposition framework. The proposed methods work for both constant Knudsen number ε and spatially variant $\varepsilon = \varepsilon(x)$ in a wide range. The high order spatial accuracy is achieved by nodal discontinuous Galerkin (NDG) finite element approaches [24], and the high order temporal accuracy is achieved by globally stiffly accurate implicit-explicit (IMEX) Runge-Kutta (RK) methods [10, 11]. A formal asymptotic analysis showing that the scheme becomes a DG method [33] with explicit RK time discretizations for the compressible Euler system in the zero limit of the Knudsen number. While for sufficiently small ε it gives rise to a local DG (LDG) discretization [5, 18, 7, 28, 6], up to $\mathcal{O}(\varepsilon^2)$, for the compressible Navier-Stokes equations.

Although it is more accurate to use kinetic models to describe physics problems, it is computationally very expensive to simulate. On the other hand, fluid descriptions, such as compressible Euler and Navier-Stokes equations, typically break down near shocks or kinetic boundary layers. In a multi-scale scenario, it is of interest to use the kinetic model only locally in regions where it is necessary, while taking the advantage of low computational cost of the fluid system elsewhere. For computational efficiency, many hybrid kinetic/fluid schemes with automatic domain decomposition criteria have been developed. Many of these criteria are based on the macroscopic quantities to pass from the hydrodynamic description to kinetic ones. They are easy to compute numerically, but they could become inaccurate near shock or boundary layers. For example, Boyd, Chen and Candler [12] proposed a criterion based on the local Knudsen number, where the kinetic description is used when the quantity is below a problem-dependent threshold value. This criterion later was used by Kolobov et al. with a discrete-velocity model of the Boltzmann equation and a kinetic scheme for the hydrodynamic equations [26], and then by Degond and Dimarco with a Monte-Carlo solver for the kinetic equation and a finite volume method for the macroscopic ones. Another criterion based on the viscous and heat fluxes of the Navier-Stokes equations, through a Grad's 13-moments expansion was introduced by Tiwari in [34]. This criterion is used with a deterministic solver for the kinetic one by Degond, Dimarco and Mieussens in [19], Tiwari, Klar and Hardt in [35, 36], Alaia and Puppo in [1] and Dimarco, Mieussens and Rispoli in [20]. Recently in [23] Filbet and Rey proposed a hybrid method based on the moment realizability criteria introduced by Levermore, Morokoff and Nadiga [27]. In this work, the criteria to/from kinetic from/to hydrodynamic regimes via macroscopic and microscopic quantities are proposed respectively. The hybrid scheme combines a central finite volume scheme using central Lax-Friedrichs fluxes [30] for the fluid equations with an asymptotic scheme with a first order IMEX discretization [22] for the kinetic ES-BGK equation.

Motivated by the criteria developed in [23], in this paper, we design a hierarchy scheme based on the NDG-IMEX developed in [37]. The domain decomposition approach can be very applied to the NDG-IMEX method naturally, as the scheme automatically becomes a fluid solver in the hydrodynamic regime (a DG scheme for the compressible Euler equations and an LDG scheme for the compressible Navier-Stokes equations). Moreover, as a new ingredient,

we propose a criterion to adaptively identify the Euler, Navier-Stokes and kinetic regimes, in which the corresponding high order numerical solvers are applied. Numerical experiments on one dimensional problems are performed to showcase the effectiveness of the new approach. Significant savings on the computational cost are observed, as compared to the full NDG-IMEX scheme for the kinetic BGK equation.

The rest of the paper is organized as follows. In Section 2, the BGK equation in a hyperbolic scaling and its micro-macro decomposition is given. In Section 3, high order AP nodal DG spatial discretization and globally stiffly accurate IMEX temporal discretizations are presented. The regime indicators are introduced. In Section 4, numerical results are performed for one dimensional problems. Conclusions are given in the final section.

2 BGK Equation and Macro-micro Formulation

We consider the BGK equation in a hyperbolic scaling:

$$\partial_t f + v \cdot \nabla_x f = \frac{1}{\varepsilon} (M_U - f) \quad (2.1)$$

where $f = f(x, v, t)$ is the distribution function of particles that depends on time $t > 0$, position $x \in \Omega_x \subset \mathbb{R}^d$ and velocity $v \in \mathbb{R}^d$ for $d \geq 1$. The parameter ε is the Knudsen number proportional to the mean free path, and M_U is the local Maxwellian defined by

$$M_U = M_U(x, v, t) = \frac{\rho(x, t)}{(2\pi T(x, t))^{d/2}} \exp\left(-\frac{|v - u(x, t)|^2}{2T(x, t)}\right). \quad (2.2)$$

ρ , u , T represent the macroscopic density, the mean velocity, and the temperature respectively. U has the components of the density, momentum and energy, which are obtained by taking the first few moments of f :

$$U := (\rho, \rho u, E)^\top = \int_{\mathbb{R}^d} \left(1, v, \frac{1}{2}|v|^2\right)^\top f(v) dv. \quad (2.3)$$

where $E = \frac{1}{2}\rho|u|^2 + \frac{d}{2}\rho T$ and the superscript \top denotes the transpose of the corresponding vector. In this paper, we use $m = m(v) := \left(1, v, \frac{1}{2}|v|^2\right)^\top$ and let $\langle g \rangle := \int_{\mathbb{R}^d} g(v) dv$. It is easy to check that $\langle m M_U \rangle = (\rho, \rho u, \frac{1}{2}\rho|u|^2 + \frac{d}{2}\rho T)^\top = U$. Hence $\langle m(M_U - f) \rangle = 0$, namely the BGK operator satisfies the conservation of mass, momentum and energy. Moreover, it enjoys the entropy dissipation: $\langle (M_U - f) \log f \rangle \leq 0$.

In the following, we briefly recall the micro-macro decomposition of (2.1), from which the compressible Euler and Navier-Stokes limits will be followed. For details, see [37]. Let us first introduce several notations. Taking $M = M_U$ for short, we use L_M^2 to denote the Hilbert space equipped with the weighted inner product

$$(f, g)_M := \langle f g M^{-1} \rangle,$$

then for any function $f \in L_M^2$, we can write $f \in L_M^2$ as

$$f = \Pi_M f + (\mathbf{I} - \Pi_M) f.$$

where $\Pi_M f$ is an orthogonal projection from L_M^2 onto $\mathcal{N} := \text{span}\{M, vM, |v|^2 M\}$, and it is explicitly given by

$$\Pi_M f = \left(\frac{1}{\rho} \langle f \rangle + \frac{\langle (v-u)f \rangle}{\rho T} \cdot (v-u) + \frac{2}{d\rho} \left(\left(\frac{|v-u|^2}{2T} - \frac{d}{2} \right) f \right) \left(\frac{|v-u|^2}{2T} - \frac{d}{2} \right) \right) M. \quad (2.4)$$

By the orthogonal project, we can decompose f into a macroscopic part M and a microscopic part εg ,

$$f := M + \varepsilon g, \quad (2.5)$$

with $\langle mg \rangle = 0$. Inserting (2.5) into (2.1) and applying the orthogonal projections Π_M and $\mathbf{I} - \Pi_M$ respectively, we will have the following macro-micro decomposed equations:

$$\partial_t U + \nabla_x \cdot F(U) + \varepsilon \nabla_x \cdot \langle vmg \rangle = 0, \quad (2.6a)$$

$$\varepsilon \partial_t g + \varepsilon (\mathbf{I} - \Pi_M)(v \cdot \nabla_x g) = -(g + (\mathbf{I} - \Pi_M)(v \cdot \nabla_x M)). \quad (2.6b)$$

where the flux $F(U) = (\rho u, \rho u \otimes u + pI, (E+p)u)^\top$ and $p = \rho T$. I is the $d \times d$ identity matrix. In a more general setting where the Knudsen number depends on the position $\varepsilon = \varepsilon(x)$, the micro-macro formulation (2.6) should be written as follows:

$$\partial_t U + \nabla_x \cdot F(U) + \nabla_x \cdot (\varepsilon(x) \langle vmg \rangle) = 0, \quad (2.7a)$$

$$\varepsilon(x) \partial_t g + (\mathbf{I} - \Pi_M) \nabla_x \cdot (\varepsilon(x) vg) = -(g + (\mathbf{I} - \Pi_M)(v \cdot \nabla_x M)). \quad (2.7b)$$

We observe that the first two terms in (2.6a) form the Euler system and eq. (2.6a) formally converges to the Euler system as $\varepsilon \rightarrow 0$. For the third term in eq. (2.6a), the leading order (ε term) will give rise to the viscous term in compressible Navier-Stokes equations. To see this, we have, from (2.6b),

$$g = -(\mathbf{I} - \Pi_M)(v \cdot \nabla_x M) + \mathcal{O}(\varepsilon) \quad (2.8)$$

and the direct computation shows that

$$\frac{(\mathbf{I} - \Pi_M)(v \cdot \nabla_x M)}{M} = \frac{1}{2} A : \left(\nabla_x u + (\nabla_x u)^\top - \frac{2}{d} (\nabla_x \cdot u) I \right) + B \cdot \frac{\nabla_x T}{\sqrt{T}} \quad (2.9)$$

where

$$A = \frac{(v-u) \otimes (v-u)}{T} - \frac{|v-u|^2}{dT} I \quad \text{and} \quad B = \left(\frac{|v-u|^2}{2T} - \frac{d+2}{2} \right) \frac{v-u}{\sqrt{T}}. \quad (2.10)$$

Therefore, we deduce that

$$g = -A : \left(\nabla_x u + (\nabla_x u)^\top - \frac{2}{d} (\nabla_x \cdot u) I \right) M - B \cdot \frac{\nabla_x T}{\sqrt{T}} M + \mathcal{O}(\varepsilon). \quad (2.11)$$

Here $X : Y = \sum_{i,j} X_{ij} Y_{ij}$ is the Frobenius inner product for matrices. As we insert the expression (2.11) into (2.6a), we obtain

$$\partial_t \begin{pmatrix} \rho \\ \rho u \\ E \end{pmatrix} + \nabla_x \cdot \begin{pmatrix} \rho u \\ \rho u \otimes u + pI \\ (E+p)u \end{pmatrix} = \varepsilon \begin{pmatrix} 0 \\ \nabla_x \cdot \sigma \\ \nabla_x \cdot (\sigma u + q) \end{pmatrix} + \mathcal{O}(\varepsilon^2) \quad (2.12)$$

where

$$\sigma = \mu D(u), \quad D(u) = \nabla_x u + (\nabla_x u)^\top - \frac{2}{d}(\nabla_x \cdot u)I \text{ and } q = \kappa \nabla_x T \quad (2.13)$$

and

$$\mu = \frac{T}{4} \langle A : AM \rangle \text{ and } \kappa = T \langle B \cdot BM \rangle.$$

We refer to [4] for more details on the derivation. The above system (2.12) is the compressible Navier-Stokes equations if we disregard high order terms $\mathcal{O}(\varepsilon^2)$. We note that when $d = 1$, $\sigma = 0$ and $\kappa = \frac{3}{2}\rho T$.

As we point out in [37], although the BGK equation shares the basic properties of hydrodynamics with the Boltzmann equation, the Navier-Stokes equations derived from those equations display different viscosity and heat conductivity coefficients [14, 15, 16]. We would remark that in this case, the ellipsoidal statistical BGK (ES-BGK) [2] operator can be used in the macro-micro decomposition framework.

3 NDG-IMEX Methods

In this section, we will briefly review the NDG-IMEX scheme developed in [37], where the nodal discontinuous Galerkin (NDG) method in space together with implicit-explicit (IMEX) Runge-Kutta (RK) time discretization is used. We will only focus on the one-dimensional case with $d = 1$, $\Omega_x = [a, b]$ and $\Omega_v = [-V_c, V_c]$ with V_c sufficiently large so that the Maxwellian defined in (2.2) can be regarded as zero outside Ω_v numerically. For simplicity, we will just consider Scheme II in [37] for the general $\varepsilon(x)$ in (2.7) here, but Scheme I can be used similarly. Extension to high dimensions will be considered later and contribute to our future work.

3.1 Semi-discrete NDG methods

Start with a partition of Ω_x , $a = x_{\frac{1}{2}} < x_{\frac{3}{2}} < \dots < x_{N_x + \frac{1}{2}} = b$. Let $I_i = [x_{i-\frac{1}{2}}, x_{i+\frac{1}{2}}]$ denote an element with its length h_i , and let $h = \max_{i=0}^{N_x} h_i$. Given any non-negative integer K , we define a finite dimensional discrete space,

$$Z_h^K = \{z \in L^2(\Omega_x) : z|_{I_i} \in P^K(I_i), \forall i\}, \quad (3.1)$$

and its vector version is denoted as \mathbf{Z}_h^K . The local space $P^K(I)$ consists of polynomials of degree at most K on I . Note that functions in Z_h^K are piecewise defined. To distinguish the left and right limits of a function $z \in Z_h^K$ at a grid point $x_{i+\frac{1}{2}}$, we let $z_{i+\frac{1}{2}}^\pm = \lim_{\Delta x \rightarrow \pm 0} z(x_{i+\frac{1}{2}} + \Delta x)$, and we also let $[z]_{i+\frac{1}{2}} = z_{i+\frac{1}{2}}^+ - z_{i+\frac{1}{2}}^-$ as the jump.

Consider the relation (2.9) in one dimension, we have

$$(\mathbf{I} - \Pi_M)(v \partial_x M) = A \frac{\partial_x T}{\sqrt{T}} M. \quad (3.2)$$

With this, the equation (2.7b) becomes

$$\varepsilon(x) \partial_t g + (\mathbf{I} - \Pi_M) \partial_x (\varepsilon(x) v g) = - \left(g + A \frac{\partial_x T}{\sqrt{T}} M \right). \quad (3.3)$$

A semi-discrete DG method for the micro-macro system (2.7) is designed as following. We seek $U_h(\cdot, t) \in \mathbf{Z}_h^K$ and $g_h(\cdot, v, t) \in Z_h^K$, such that $\forall \phi, \psi \in Z_h^K$ and $\forall i$,

$$\begin{aligned} \int_{I_i} \partial_t U_h \phi dx &= \int_{I_i} (F(U_h) + \varepsilon(x) \langle vmg_h \rangle) \frac{d\phi(x)}{dx} dx - \hat{F}_{i+\frac{1}{2}} \phi_{i+\frac{1}{2}}^- + \hat{F}_{i-\frac{1}{2}} \phi_{i-\frac{1}{2}}^+ \\ &\quad - \varepsilon(x_{i+\frac{1}{2}}) \langle \widehat{vmg_h} \rangle_{i+\frac{1}{2}} \phi_{i+\frac{1}{2}}^- + \varepsilon(x_{i-\frac{1}{2}}) \langle \widehat{vmg_h} \rangle_{i-\frac{1}{2}} \phi_{i-\frac{1}{2}}^+, \end{aligned} \quad (3.4a)$$

$$\int_{I_i} \varepsilon(x) \partial_t g_h \psi dx + \int_{I_i} (\mathbf{I} - \Pi_{M_h}) (\mathcal{D}_{h,1}(\varepsilon(x) v g_h)) \psi dx = - \int_{I_i} g_h \psi dx - \int_{I_i} A_h \frac{r_h}{\sqrt{T_h}} M_h \psi dx, \quad (3.4b)$$

Here $M_h = M_{U_h}$ according to (2.2). $\mathcal{D}_{h,1}(\varepsilon(x) v g_h)(\cdot, v, t) \in Z_h^K$ and $r_h \in Z_h^K$ are approximations of the spatial derivative of $\varepsilon(x) v g$ and T , respectively, based on DG discretizations. Particularly, $\forall \psi \in Z_h^K$ and $\forall i$,

$$\int_{I_i} \mathcal{D}_{h,1}(\varepsilon(x) v g_h) \psi dx := - \int_{I_i} \varepsilon(x) v g_h \frac{d\psi}{dx} dx + \varepsilon(x_{i+\frac{1}{2}}) \langle \widetilde{v g_h} \rangle_{i+\frac{1}{2}} \psi_{i+\frac{1}{2}}^- - \varepsilon(x_{i-\frac{1}{2}}) \langle \widetilde{v g_h} \rangle_{i-\frac{1}{2}} \psi_{i-\frac{1}{2}}^+, \quad (3.5)$$

where $\widetilde{v g}$ is an upwind numerical flux consistent to vg ,

$$\widetilde{v g} := \begin{cases} v g^-, & \text{if } v > 0, \\ v g^+, & \text{if } v < 0, \end{cases} \quad (3.6)$$

and $\forall \varphi \in Z_h^K$ and $\forall i$

$$\int_{I_i} r_h \varphi dx = - \int_{I_i} T_h \frac{d\varphi}{dx} dx + \hat{T}_{h,i+\frac{1}{2}} \varphi_{i+\frac{1}{2}}^- - \hat{T}_{h,i-\frac{1}{2}} \varphi_{i-\frac{1}{2}}^+. \quad (3.7)$$

Here T_h , a macroscopic quantity, and A_h can be obtained from U_h based on the energy E under (2.3) and (2.10) respectively. The numerical flux $\hat{F} = \hat{F}(U_h^-, U_h^+)$ in (3.4a) is taken to be the global Lax-Friedrichs flux [17]. Here the subscripts $i \pm \frac{1}{2}$ are temporarily omitted for simplicity. We take the hatted fluxed $\langle \widehat{vmg} \rangle$ and \hat{T} as the central fluxes $\langle \widehat{vmg} \rangle = \langle vm(g^- + g^+) \rangle / 2$, $\hat{T} = (T^+ + T^-) / 2$, while the alternating right-left and central fluxes introduced in [37] can also be used.

We further use the nodal basis to represent functions in the discrete space Z_h^K , and approximating the integrals in the schemes by numerical quadratures. Note that the discrete space $Z_h^K|_{I_i}$ is simply $P^K(I_i)$. We particularly choose the local nodal basis (also called Lagrangian basis) $\{\phi_i^k(x)\}_{k=0}^K$ associated with the $K+1$ Gaussian quadrature points $\{x_i^k\}_{k=0}^K$ on I_i , defined as below

$$\phi_i^k(x) \in P^K(I_i), \quad \text{and} \quad \phi_i^k(x_i^{k'}) = \delta_{kk'}, \quad k, k' = 0, 1, \dots, K. \quad (3.8)$$

Here $\delta_{kk'}$ is the Kronecker delta function. We further let $\{\omega_k\}_{k=0}^K$ denote the corresponding quadrature weights on the reference element $(-\frac{1}{2}, \frac{1}{2})$.

With the nodal basis functions, (3.4)-(3.5) and (3.7) can be equivalently stated with the test functions ϕ, ψ both being taken as $\phi_i^k, k = 0, 1, \dots, K$. We also replace all the integral terms in (3.4)-(3.5) and (3.7) by their numerical integrations based on $(K+1)$ -point Gaussian

quadrature. The scheme now becomes: find $U_h(\cdot, t) \in \mathbf{Z}_h^K$ and $g_h(\cdot, v, t) \in Z_h^K$, with $U_h(x, t)|_{I_i} = \sum_{k=0}^K U_i^k(t) \phi_i^k(x)$, $g_h(x, v, t)|_{I_i} = \sum_{k=0}^K g_i^k(v, t) \phi_i^k(x)$, such that $\forall i, k$,

$$\begin{aligned} \omega_k h_i \frac{dU_i^k}{dt} = & \sum_{k'=0}^K \omega_{k'} h_i F(U_i^{k'}) \frac{d\phi_i^k(x)}{dx} \Big|_{x=x_i^{k'}} - \hat{F}_{i+\frac{1}{2}} \phi_i^k(x_{i+\frac{1}{2}}^-) + \hat{F}_{i-\frac{1}{2}} \phi_i^k(x_{i-\frac{1}{2}}^+) \\ & + \sum_{k'=0}^K \omega_{k'} h_i \varepsilon(x_i^{k'}) \langle v m g_i^{k'} \rangle \frac{d\phi_i^k(x)}{dx} \Big|_{x=x_i^{k'}} - \varepsilon(x_{i+\frac{1}{2}}) \langle \widehat{v m g_h} \rangle_{i+\frac{1}{2}} \phi_i^k(x_{i+\frac{1}{2}}^-) \\ & + \varepsilon(x_{i-\frac{1}{2}}) \langle \widehat{v m g_h} \rangle_{i-\frac{1}{2}} \phi_i^k(x_{i-\frac{1}{2}}^+), \end{aligned} \quad (3.9a)$$

$$\begin{aligned} \varepsilon(x_i^k) \omega_k h_i \partial_t g_i^k = & (\mathbf{I} - \Pi_i^k) \left(v \sum_{k'=0}^K \omega_{k'} h_i \varepsilon(x_i^{k'}) g_i^{k'} \frac{d\phi_i^k(x)}{dx} \Big|_{x=x_i^{k'}} - \varepsilon(x_{i+\frac{1}{2}}) \langle \widetilde{v g_h} \rangle_{i+\frac{1}{2}} \phi_i^k(x_{i+\frac{1}{2}}^-) \right. \\ & \left. + \varepsilon(x_{i-\frac{1}{2}}) \langle \widetilde{v g_h} \rangle_{i-\frac{1}{2}} \phi_i^k(x_{i-\frac{1}{2}}^+) \right) - \omega_k h_i g_i^k + A_i^k \omega_k h_i r_i^k M_i^k / \sqrt{T_i^k}, \end{aligned} \quad (3.9b)$$

$$\omega_k h_i r_i^k = - \sum_{k'=0}^K \omega_{k'} h_i T_i^{k'} \frac{d\phi_i^k(x)}{dx} \Big|_{x=x_i^{k'}} + \hat{T}_{h,i+\frac{1}{2}} \phi_i^k(x_{i+\frac{1}{2}}^-) - \hat{T}_{h,i-\frac{1}{2}} \phi_i^k(x_{i-\frac{1}{2}}^+). \quad (3.9c)$$

Here $M_i^{k'} = M_h|_{x=x_i^{k'}}$, $\Pi_i^k = \Pi_{M_i^k}$ and $r_i^k = r_h|_{x=x_i^k}$. And the nodal values of $T_i^k = T_h|_{x=x_i^k}$ and $A_i^k = A_h|_{x=x_i^k}$ are obtained from U_i^k based on (2.3) and (2.10).

To the end, we also need to discretize the v -direction. In this work, $\Omega_v = [-V_c, V_c]$ is discretized uniformly with N_v points, $\{v_j\}_{j=1}^{N_v}$. For the integration in v , the mid-point rule is applied, which is spectrally accurate for smooth functions with periodic boundary conditions or with a compact support [13]. Such approach does not preserve the conservation properties of mass, moment and energy at the discrete level as in [29], yet in [37] we have found it is a sufficiently accurate discretization for all test cases that we have performed.

3.2 IMEX time discretization

Now we will formulate the IMEX RK time discretizations for the semi-discrete schemes introduced in Section 3.1. First we rewrite the scheme in a compact form as follows. Find $U_h(\cdot, t) \in \mathbf{Z}_h^K$, $g_h(\cdot, v, t), r_h(\cdot, t) \in Z_h^K$, such that $\forall \phi, \psi, \varphi \in Z_h^K$ and $\forall i$,

$$(\partial_t U_h, \phi) + F_h(U_h, \phi) = D_h(\varepsilon(x) g_h, \phi), \quad (3.10a)$$

$$(\varepsilon(x) \partial_t g_h, \psi) + b_{h,v}(\varepsilon(x) g_h, \psi) = s_h^{(1)}(g_h, \psi) + s_{h,v}^{(2)}(U_h, r_h, \psi), \quad (3.10b)$$

$$(r_h, \varphi) = H_h(U_h, \varphi), \quad (3.10c)$$

where

$$F_h(U_h, \phi) = - \int_{\Omega_x} F(U_h) \frac{d\phi(x)}{dx} dx - \sum_i \hat{F}_{h,i+\frac{1}{2}}[\phi]_{i+\frac{1}{2}}, \quad (3.11a)$$

$$D_h(\varepsilon(x)g_h, \phi) = \int_{\Omega_x} \varepsilon(x) \langle vmg_h \rangle \frac{d\phi(x)}{dx} dx + \sum_i \varepsilon(x_{i+\frac{1}{2}}) \widehat{\langle vmg_h \rangle}_{i+\frac{1}{2}}[\phi]_{i+\frac{1}{2}}, \quad (3.11b)$$

$$b_{h,v}(\varepsilon(x)g_h, \psi) = \int_{\Omega_x} (\mathbf{I} - \Pi_{M_h}) \mathcal{D}_{h,1}(\varepsilon(x)vg_h) \psi dx, \quad (3.11c)$$

$$s_h^{(1)}(g_h, \psi) = - \int_{\Omega_x} g_h \psi dx, \quad s_{h,v}^{(2)}(U_h, r_h, \psi) = - \int_{\Omega_x} A_h \frac{r_h}{\sqrt{T_h}} M_h \psi dx, \quad (3.11d)$$

$$H_h(U_h, \varphi) = - \left(\int_{\Omega_x} T_h \frac{d\varphi}{dx} dx + \sum_i \hat{T}_{h,i+\frac{1}{2}}[\varphi]_{i+\frac{1}{2}} \right) \Big|_{T_h=T_h(U_h)}. \quad (3.11e)$$

High order globally stiffly accurate IMEX schemes can be characterized by a double Butcher Tableau

$$\begin{array}{c|c} \tilde{c} & \tilde{A} \\ \hline & \tilde{b}^\top \end{array} \quad \begin{array}{c|c} c & A \\ \hline & b^\top \end{array}, \quad (3.12)$$

where $\tilde{A} = (\tilde{a}_{ij})$ is an $s \times s$ lower triangular matrix with zero diagonal for an explicit scheme, and $A = (a_{ij})$ is an $s \times s$ lower triangular matrix with the diagonal entries not all being zero for a diagonally implicit RK (DIRK) method. The coefficients \tilde{c} and c are given by the standard relations

$$\tilde{c}_i = \sum_{j=1}^{i-1} \tilde{a}_{ij}, \quad c_i = \sum_{j=1}^i a_{ij}, \quad (3.13)$$

and vectors $\tilde{b} = (\tilde{b}_j)$ and $b = (b_j)$ represent the quadrature weights for internal stages of the RK method. The IMEX RK scheme is defined to be *globally stiffly accurate* if $\tilde{c}_s = c_s = 1$ and $a_{sj} = b_j$, $\tilde{a}_{sj} = \tilde{b}_j$, $\forall j = 1, \dots, s$.

Now the fully-discrete scheme using the Butcher notation can be written as follows. Given $U_h^n \in \mathbf{Z}_h^K$ and $g_h^n \in Z_h^K$, we look for $U_h^{n+1} \in \mathbf{Z}_h^K$ and $g_h^{n+1} \in Z_h^K$, such that $\forall \phi, \psi \in Z_h^K$,

$$(U_h^{n+1}, \phi) = (U_h^n, \phi) - \Delta t \sum_{l=1}^s \tilde{b}_l \left(F_h(U_h^{(l)}, \phi) - D_h(\varepsilon(x)g_h^{(l)}, \phi) \right), \quad (3.14a)$$

$$(\varepsilon(x)g_h^{n+1}, \psi) = (\varepsilon(x)g_h^n, \psi) - \Delta t \sum_{l=1}^s \tilde{b}_l b_{h,v}(\varepsilon(x)g_h^{(l)}, \psi) + \Delta t \sum_{l=1}^s b_l \left(s_h^{(1)}(g_h^{(l)}, \psi) + s_{h,v}^{(2)}(U_h^{(l)}, r_h^{(l)}, \psi) \right). \quad (3.14b)$$

Here the approximations at the internal stages of one RK step, $U_h^{(l)} \in \mathbf{Z}_h^K$ and $g_h^{(l)}, r_h^{(l)} \in Z_h^K$

with $l = 1, \dots, s$, satisfy

$$\left(U_h^{(l)}, \phi \right) = (U_h^n, \phi) - \Delta t \sum_{j=1}^{l-1} \tilde{a}_{lj} \left(F_h(U_h^{(j)}, \phi) - D_h(\varepsilon(x)g_h^{(j)}, \phi) \right), \quad (3.15a)$$

$$\left(\varepsilon(x)g_h^{(l)}, \psi \right) = (\varepsilon(x)g_h^n, \psi) - \Delta t \sum_{j=1}^{l-1} \tilde{a}_{lj} b_{h,v}(\varepsilon(x)g_h^{(j)}, \psi) + \Delta t \sum_{j=1}^l a_{lj} \left(s_h^{(1)}(g_h^{(j)}, \psi) + s_{h,v}^{(2)}(U_h^{(j)}, r_h^{(j)}, \psi) \right), \quad (3.15b)$$

$$(r_h^{(l)}, \varphi) = H_h(U_h^{(l)}, \varphi), \quad (3.15c)$$

for any $\phi, \psi, \varphi \in Z_h^K$. One can solve the IMEX scheme in a stage-by-stage fashion for $l = 1, \dots, s$, that is, we first solve $U_h^{(l)}$ explicitly from the equation (3.15a), then plug $U_h^{(l)}$ into (3.15c) to solve $r_h^{(l)}$, and finally solve $g_h^{(l)}$ from (3.15b).

The third order IMEX scheme we use in our simulations is the globally stiffly accurate ARS(4, 4, 3) scheme [3] with a double Butcher Tableau

$$\begin{array}{c|ccccc|ccccc} 0 & 0 & 0 & 0 & 0 & 0 & 0 & 0 & 0 & 0 & 0 \\ 1/2 & 1/2 & 0 & 0 & 0 & 0 & 1/2 & 0 & 1/2 & 0 & 0 \\ 2/3 & 11/18 & 1/18 & 0 & 0 & 0 & 2/3 & 0 & 1/6 & 1/2 & 0 \\ 1/2 & 5/6 & -5/6 & 1/2 & 0 & 0 & 1/2 & 0 & -1/2 & 1/2 & 0 \\ 1 & 1/4 & 7/4 & 3/4 & -7/4 & 0 & 1 & 0 & 3/2 & -3/2 & 1/2 \\ \hline & 1/4 & 7/4 & 3/4 & -7/4 & 0 & & 0 & 3/2 & -3/2 & 1/2 \end{array} \quad (3.16)$$

For the fully discrete DG-IMEX scheme (3.14)-(3.15), with operators specified in (3.11), the Proposition 3.4 in [37] has shown that, for $0 < \varepsilon \ll 1$, the scheme is asymptotically equivalent, up to $\mathcal{O}(\varepsilon^2)$, to a local DG (LDG) method in its nodal form for the compressible Navier-Stokes equations

$$\partial_t \begin{pmatrix} \rho \\ \rho u \\ E \end{pmatrix} + \partial_x \begin{pmatrix} \rho u \\ \rho u^2 + pI \\ (E + p)u \end{pmatrix} = \varepsilon \partial_x \begin{pmatrix} 0 \\ 0 \\ \frac{3}{2} \rho T \partial_x T \end{pmatrix}. \quad (3.17)$$

and the LDG scheme evolved in time by an explicit RK method characterized by a Butcher table \tilde{A} , \tilde{b} and \tilde{c} in (3.12) is defined as follows: find $U_h^{n+1}(\cdot, t), U_h^{(l)} \in \mathbf{Z}_h^K$ and $r_h^{(l)}(\cdot, t) \in Z_h^K$ with $l = 1, \dots, s$, such that $\forall \phi, \varphi \in Z_h^K$,

$$(U_h^{n+1}, \phi) = (U_h^n, \phi) - \Delta t \sum_{l=1}^s \tilde{b}_l \left(F_h(U_h^{(l)}, \phi) - \varepsilon F_h^{(vis)}(U_h^{(l)}, r_h^{(l)}, \phi) \right), \quad (3.18)$$

with

$$\left(U_h^{(l)}, \phi \right) = (U_h^n, \phi) - \Delta t \sum_{j=1}^{l-1} \tilde{a}_{lj} \left(F_h(U_h^{(j)}, \phi) - \varepsilon F_h^{(vis)}(U_h^{(j)}, r_h^{(j)}, \phi) \right), \quad (3.19)$$

and

$$(r_h^{(l)}, \varphi) = - \sum_i \left(\int_{I_i} T_h^{(l)} \frac{d\varphi}{dx} dx + \hat{T}_{h,i+\frac{1}{2}}^{(l)} [\varphi]_{i+\frac{1}{2}} \right). \quad (3.20)$$

Its nodal form can be similarly defined as in Section 3.1 and is omitted for brevity. When $\varepsilon = 0$, if we omit the ε terms in (3.18) and (3.19), it becomes a RK DG scheme for the compressible Euler system.

3.3 Regime indicators

In this section, we will introduce the regime indicators to group all the computational cells into three classes: (I) Euler regime, (II) Navier-Stokes (NS) regime, (III) kinetic regime. We will start all cells in the kinetic regime unless the initial conditions are apparently in the fluid regime. We have the criteria for both directions: from/to kinetic to/from hydrodynamic regimes. In particular, we use macroscopic quantities to determine when the hydrodynamic description breaks down, and use microscopic ones to determine when the kinetic description is not necessary and a hydrodynamic description would be sufficient. Moreover, we also distinguish between compressible Euler and Navier-Stokes in the hydrodynamics regime, where a finer criteria is proposed.

Before we start, we first follow [23] to introduce several notations. For simplicity, in the following, we consider the problem in the one-dimensional case where $d = 1$. We use the short hand notation for the rescaled microscopic velocity $V(v) = \frac{v-u}{\sqrt{T}}$, then A and B defined in (2.10) can be written as $A = 0$ and $B(V) = \frac{1}{2} (V^2 - 3) V$. We let $\bar{B} := \frac{1}{\rho} \int_{\mathbb{R}} B(V) f(v) dv$.

3.3.1 From fluid to kinetic: The moment realizability criterion

Following [27, 23], we define the moment realizability matrix as

$$\mathbf{M} := \frac{1}{\rho} \int_{\mathbb{R}} \mathbf{m} \otimes \mathbf{m} f(v) dv, \quad (3.21)$$

where \mathbf{m} is the collisional invariant vector for $V = (v - u)/\sqrt{T}$,

$$\mathbf{m} := \left(1, V, \frac{1}{\sqrt{2}} (V^2 - 1) \right). \quad (3.22)$$

From the properties of the moments defined in (2.3), we have

$$\begin{aligned} \mathbf{M} &= \frac{1}{\rho} \int_{\mathbb{R}} \begin{pmatrix} 1 & V & \frac{1}{\sqrt{2}} (V^2 - 1) \\ V & V^2 & \frac{1}{\sqrt{2}} (V^2 - 1) V \\ \frac{1}{\sqrt{2}} (V^2 - 1) & \frac{1}{\sqrt{2}} (V^2 - 1) V & \frac{1}{2} (V^2 - 1)^2 \end{pmatrix} f(v) dv \\ &= \begin{pmatrix} 1 & 0 & 0 \\ 0 & 1 & \frac{1}{\sqrt{2}} \bar{B} \\ 0 & \frac{1}{\sqrt{2}} \bar{B} & \bar{C} \end{pmatrix} \end{aligned} \quad (3.23)$$

where \bar{C} is the dimensionless fourth order moment of f :

$$\bar{C} = \frac{1}{2\rho} \int_{\mathbb{R}} (V^2 - 1)^2 f(v) dv.$$

Now let us consider different orders for the approximation of f with respect to ε . The values of \bar{B} and \bar{C} can then be explicitly determined.

- Zeroth order: Compressible Euler system.

We have $f = M_U$, since \bar{B} only involves odd, centered moments of f , so that $\bar{B} = 0$. Direct computation shows that $\bar{C} = 1$. In this case, \mathbf{M} is the identity matrix, all the eigenvalues are 1, we denote it as $\nu_{Euler} = 1$.

- First order: Compressible Navier-Stokes system.

We have $f = M_U + \varepsilon g = M_U - \varepsilon A \frac{T_x}{\sqrt{T}} M$, with analytical expression for the projection term defined in (2.9). And we can find that $\bar{B} = -\varepsilon \frac{\kappa}{\rho T^{3/2}} \nabla_x T$, where $q = \kappa \nabla_x T$ is the heat flux. For \bar{C} , using symmetry arguments, we still have $\bar{C} = 1$. For the matrix \mathbf{M} , beside one eigenvalue to be 1, the other two eigenvalues would be $1 \pm \bar{B}$. We denote the largest absolute eigenvalue for the compressible Navier-Stokes equations as $\nu_{NS} = 1 + |\bar{B}| = 1 + \varepsilon \frac{\kappa}{\rho T^{3/2}} |\nabla_x T|$.

- Second order: Burnett equations.

The second order Burnett equations will be used as a reference for the kinetic equation, when the fluid is far away from the thermal equilibrium. It would be complicate to derive the explicit expression for \bar{B} under the micro-macro decomposition framework up to second order. Instead, we directly use the one obtained from Chapman-Enskog expansion as in [23]. Since $D(u) = 0$, here the expression for \bar{B} would be

$$\bar{B} = -\varepsilon \frac{\kappa}{\rho T^{3/2}} T_x - \varepsilon^2 \frac{\mu^2}{\sqrt{T}} \left(\frac{25}{6} u_x T - \frac{5}{3} (T u_{xx} + 7 u_x T_x) \right). \quad (3.24)$$

Similarly, beside 1 is one eigenvalue of \mathbf{M} , the other two eigenvalues are $1 \pm \bar{B}$, so that we denote $\nu_B = 1 + |\bar{B}|$ with \bar{B} in (3.24).

A criterion to determine whether a hydrodynamic description breaks down is to find out the deviation of the eigenvalues in the corresponding fluid models away from the reference eigenvalue which we denoted as ν_B . We propose a criterion with the following two steps:

- **Step 1:** If one cell is not in the kinetic regime, then if it is in the Euler regime, it will be classified as the NS regime if $|\nu_B - \nu_{Euler}| > \eta_0$.
- **Step 2:** For all the cells in the NS regime (with those from the Euler regime in Step 1), if $|\nu_B - \nu_{NS}| > \eta_1$, they will be classified as the kinetic regime.

The best choice of the thresholds η_0 and η_1 is problem dependent. In our numerical tests, we all take $\eta_0 = 10^{-2}$ and $\eta_1 = 10^{-1}$. In order to avoid classifying a smooth extremum (where T_x and u_x might both be zero) as the Euler regime (which may not be physically accurate), we propose to change a cell from the Euler regime into the NS regime if both of its neighbors are in the NS regime.

Remark 3.1. In our numerics, the first and second derivatives, such as T_x , u_x and u_{xx} when computing the eigenvalues, are approximated by a DG or LDG discretization with central fluxes.

3.3.2 From kinetic to fluid

The criterion in this direction would simply be a comparison between the kinetic density $f = M + \varepsilon g$ and the truncated distribution f_k whose moments match those of f and k is the order of the macroscopic model. In particular, a kinetic description will be changed to a hydrodynamic closure of k if

$$\|f(t, x, \cdot) - f_k(t, x, \cdot)\|_{L_M^2} \leq \delta_0, \quad (3.25)$$

with a weighted L^2 norm defined as $\|\cdot\|_{L_M^2} = (\int_{\mathbb{R}} |\cdot|^2 / M_U dv / \rho)^{1/2}$. For example, $f_1(t, x, v) = M$ and $\|f(t, x, v) - f_1(t, x, v)\|_{L_M^2} = \varepsilon \|g(t, x, v)\|_{L_M^2}$, while $f_2(t, x, v) = M - \varepsilon A \frac{T_x}{\sqrt{T}} M$ and $\|f(t, x, v) - f_2(t, x, v)\|_{L_M^2} = \varepsilon \|g(t, x, v) + A \frac{T_x}{\sqrt{T}} M\|_{L_M^2}$. The criterion is implemented in the following two steps:

- **Step 1:** For a cell not in the Euler regime (including both NS and kinetic), if $\varepsilon \|g(t, x, v)\|_{L_M^2} < \delta_0$, it is added to the Euler regime.
- **Step 2:** Otherwise, if it is in the kinetic regime and $\varepsilon \|g(t, x, v) + A \frac{T_x}{\sqrt{T}} M\|_{L_M^2} < \delta_0$, it is added to the NS regime.

In our numerical tests, we take $\delta_0 = 10^{-3}$.

Remark 3.2. In the hydrodynamic part including Euler and NS regimes, we only have the information of U , while in the kinetic regime both U and g are solved. In order to match the interfaces between the fluid and kinetic regimes, g needs to be recovered in the fluid regime as the value at the thermal equilibrium $g = -A \frac{T_x}{\sqrt{T}} M$.

Remark 3.3. Our hierarchical algorithm with regime indicators realizes an adaptive seamless coupling between hydrodynamic and kinetic solvers at different levels. The scheme can be briefly sketched as follows:

- Initially at $T = 0$ we start with all cells to be kinetic unless the initial conditions are apparently to be fluid. For a high order Runge-Kutta method, the criteria are only applied at the beginning of each time step.
- At each intermediate stage from time level t^n to t^{n+1} , we solve the Euler regime with RK DG method, the NS regime with LDG method and the kinetic regime with the NDG-IMEX method as described in Section 3.1 and Section 3.2. In all computational cells, macroscopic information U are stored and being updated, while the microscopic components g is stored and computed only in kinetic regimes. At boundary elements on hydrodynamic regimes (Euler or Navier-Stokes) border with the kinetic ones, we let $g = -A \frac{T_x}{\sqrt{T}} M$ as the boundary condition for microscopic component in kinetic regimes.

We remark that the seamless coupling of different solvers are due to the compactness property of the DG method and the asymptotic equivalence of the kinetic solver with macroscopic ones. In particular, schemes on all three regimes are under the NDG-IMEX framework; the NDG-IMEX scheme is asymptotically equivalent to the DG and LDG scheme for Euler and Navier-Stokes systems. The macroscopic ones avoid computing several microscopic terms, leading to significant computational savings.

4 Numerical Examples

In this section, we will apply the regime indicators to the NDG-IMEX scheme for the micro-macro decomposed BGK equation (2.6) with constant ε , and (2.7) with variable $\varepsilon(x)$. We take the third order NDG-IMEX scheme with 3-point Gauss quadrature, corresponding to a Lagrangian polynomial basis of degree 2. The corresponding DG and LDG schemes in the compressible Euler and Navier-Stokes regimes are also third order. The time step is chosen as

$\Delta t = CFLh / \max(\Lambda, V_c)$, where $CFL = 0.05$ and $\Lambda = \| |u| + \sqrt{\gamma T} \|_\infty$ is the maximal absolute eigenvalue of $\partial F(U) / \partial U$ over the spatial domain. The velocity domain $\Omega = [-V_c, V_c]$ is set to be large enough. The TVB limiter with the parameter $M_{tvb} = 1$ is used and is only applied on U_h .

We will consider three different hierarchy schemes, where the hydrodynamic regime may contain only the Euler regime, the NS regime, or both the Euler and NS regimes, which we will denote as Euler-Kinetic, NS-Kinetic and Euler-NS-Kinetic.

4.1 Sod problem

First we consider the sod shock tube problem with initial conditions to be

$$(\rho, u, T) = \begin{cases} (1, 0, 1) & \text{if } x < 0.5 \\ (0.125, 0, 0.8) & \text{if } x > 0.5. \end{cases}$$

on the domain $[-0.2, 1.2]$, $v \in [-4.5, 4.5]$.

We report the results for $\varepsilon = 10^{-2}$ in Figure 4.1 and for $\varepsilon = 10^{-3}$ in Figure 4.2, for Euler-kinetic, NS-kinetic and Euler-NS-kinetic at time $t = 0.2$. Here the hybrid schemes for all three cases are computed with 50 cells, while the reference kinetic solution and fluid solution are computed with 200 cells. The TVB limiter is used with the parameter to be 1. It is observed that in regions where the hydrodynamic and kinetic solutions differ from each other, the kinetic solver is turned on and the hybrid solutions approximate the reference kinetic solutions well. The results for all three cases match each other very well. NS-kinetic has less kinetic cells than Euler-kinetic. The Euler-NS-kinetic scheme with all three regimes together shows that NS regime well connects the Euler and kinetic regimes.

For this problem, we also compare the computational cost for different indicators, and also the full kinetic scheme. In Table 4.1, we can see that Euler-NS-kinetic can save 72% for $\varepsilon = 10^{-2}$ and 87% for $\varepsilon = 10^{-3}$ as compared to the full kinetic scheme, while NS-kinetic saves 74% for $\varepsilon = 10^{-2}$ and 85% for $\varepsilon = 10^{-3}$. Euler-kinetic is a little higher, but still 55% for $\varepsilon = 10^{-2}$ and 70% for $\varepsilon = 10^{-3}$. This is due to that the kinetic solution is very close to the Euler solution, especially when $\varepsilon = 10^{-3}$, so the regime indicators are very efficient for this problem. The Euler-NS-kinetic performs almost the same as the NS-kinetic one, costing a little higher for $\varepsilon = 10^{-2}$ and a little lower for $\varepsilon = 10^{-3}$.

Table 4.1: Comparison of the computational time (seconds) for different indicators. Sod problem.

method	Euler-NS-kinetic	NS-kinetic	Euler-kinetic	Full kinetic
$\varepsilon = 10^{-2}$	8.38	7.81	13.40	30.19
$\varepsilon = 10^{-3}$	3.78	4.28	8.28	28.57

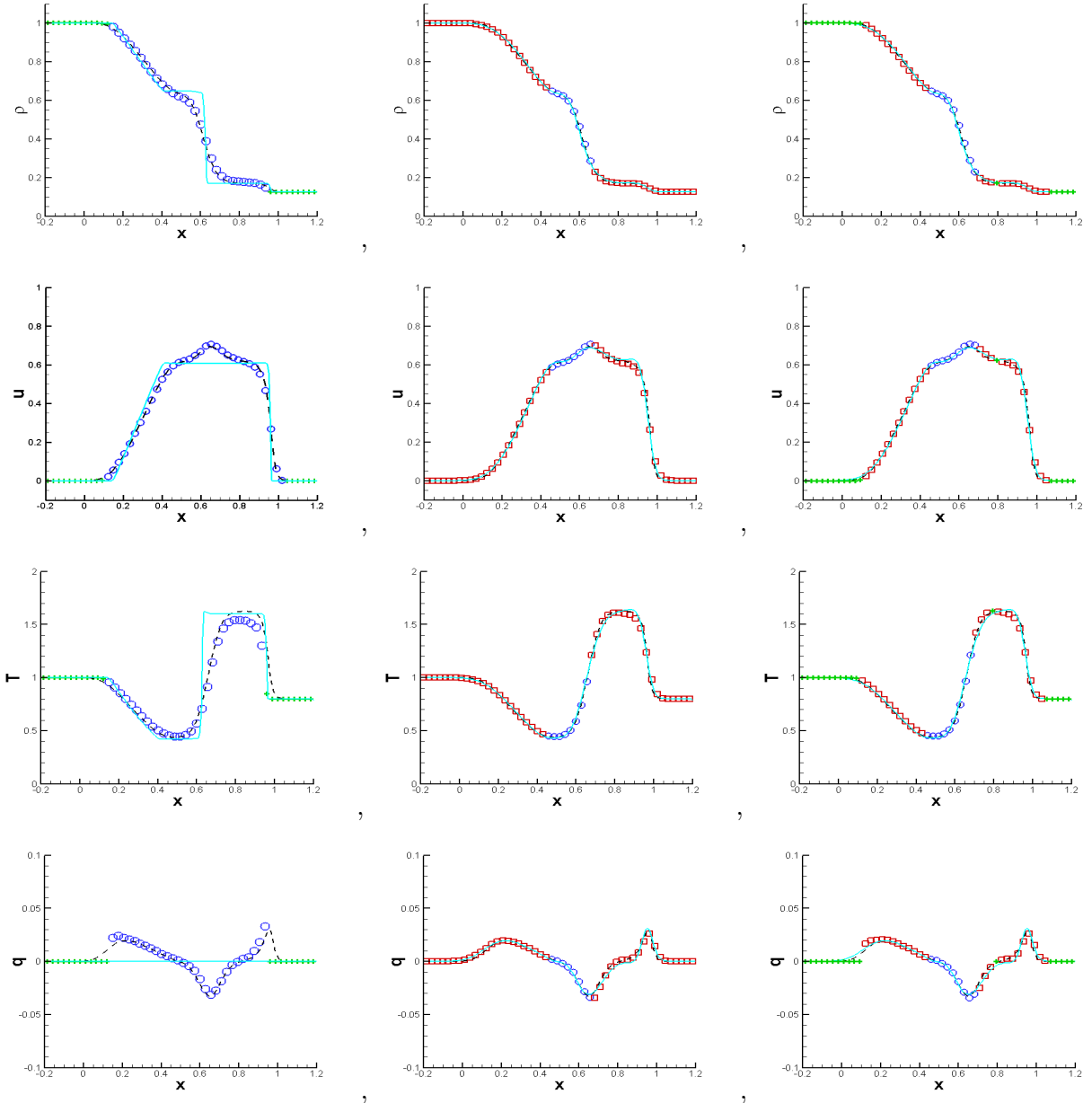


Figure 4.1: Sod problem at time $t = 0.2$ on the domain $[-0.2, 1.2] \times [-4.5, 4.5]$. Symbols: $N_x = 50$ and $N_v = 100$ with NDG3. From left to right: Euler-kinetic, NS-kinetic and Euler-NS-kinetic. From top to bottom, the density ρ , the mean velocity u , the temperature T and the heat flux q . Symbols: ‘+’ is Euler, circle is kinetic. Solid line: the Euler reference solution for Euler-kinetic and the NS reference solution for the other two. Dashed line: the kinetic reference solution. $\varepsilon = 10^{-2}$.

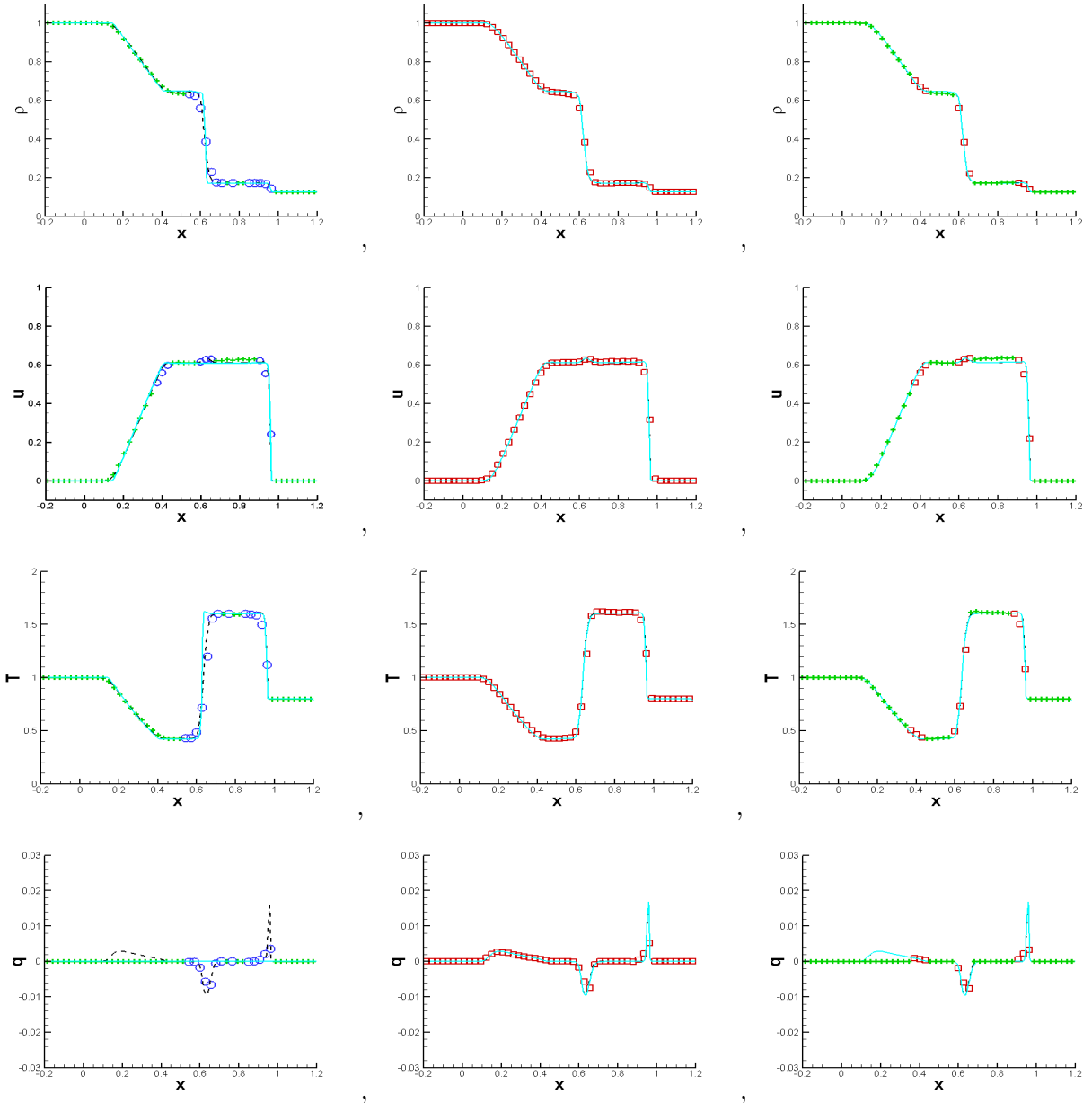


Figure 4.2: Sod problem at time $t = 0.2$ on the domain $[-0.2, 1.2] \times [-4.5, 4.5]$. Symbols: $N_x = 50$ and $N_v = 100$ with NDG3. From left to right: Euler-kinetic, NS-kinetic and Euler-NS-kinetic. From top to bottom, the density ρ , the mean velocity u , the temperature T and the heat flux q . Symbols: ‘+’ is Euler, circle is kinetic. Solid line: the Euler reference solution for Euler-kinetic and the NS reference solution for the other two. Dashed line: the kinetic reference solution. $\varepsilon = 10^{-3}$.

4.2 Blast wave problem

For the blast wave problem, the initial condition is given by

$$(\rho, u, T) = \begin{cases} (1, 1, 2) & \text{if } x < 0.2 \\ (1, 0, 0.25) & \text{if } 0.2 \leq x \leq 0.8 \\ (1, -1, 2) & \text{if } x > 0.8. \end{cases}$$

with reflective boundary condition in the x direction on the domain $[0, 1] \times [-9, 9]$.

Similarly the hybrid scheme is computed with 50 cells, while the reference kinetic solution and fluid solution are computed with 200 cells. The TVB limiter is used with the parameter to be 1. Here we report the results for $\varepsilon = 10^{-2}$ and $\varepsilon = 10^{-3}$ for Euler-NS-kinetic in Figures 4.3 and 4.4, respectively.

For this problem, when $\varepsilon = 10^{-2}$, the kinetic solution deviate slightly away from the fluid solution, and most computational cells are assigned into the kinetic regime. However, when ε becomes smaller, that is when $\varepsilon = 10^{-3}$, the kinetic solution is getting close to the hydrodynamic solution, it can be observed from Figure 4.4 that the Euler and NS solvers are turned on in larger regions, leading to computational savings. If one compares Figure 4.4, “best” solvers that well balance computational effectiveness (in capturing reference solutions) and efficiency (in saving computational time) are adaptively chosen by the criteria.

Similar to the Sod problem, we compare the computational cost for the blast wave problem in Table 4.2 for three different hierarchy schemes. As we can see, when $\varepsilon = 10^{-2}$, since the solution is mostly in the kinetic regime. Euler-NS-kinetic and NS-kinetic only save around 10% \sim 15%, while Euler-kinetic takes even more computational time than the full kinetic scheme. Also the computational time of Euler-NS-kinetic is slightly more than that of the NS-kinetic. This is due to the fact that computing the regime indicators takes extra computational time. When $\varepsilon = 10^{-3}$, the solution becomes closer to the NS solution, Euler-NS-kinetic and NS-kinetic can save up to 80%, while Euler-kinetic can only save around 60%. Also Euler-NS-kinetic takes more time than NS-kinetic. For the 1D problem, the compressible Navier-Stokes equations (3.17) has only one extra term than the compressible Euler equations. We might have taken slightly more time to compute the regime indicators and the logic decisions for the Euler-NS-kinetic approach, while computing the extra term does not take much time for 1D cases. We would expect that the savings of the Euler-NS-kinetic would become significant for high dimensional problems.

Table 4.2: Comparison of the computational cost (seconds) for different indicators. Blast wave problem.

method	Euler-NS-kinetic	NS-kinetic	Euler-kinetic	Full kinetic
$\varepsilon = 10^{-2}$	85.74	80.98	102.42	96.72
$\varepsilon = 10^{-3}$	17.22	16.77	37.97	98.72

4.3 Mixed regime problem

We consider an example with a variable $\varepsilon(x)$,

$$\varepsilon(x) = \varepsilon_0 + \frac{1}{2} \left(\tanh(1 - a_0 x) + \tanh(1 + a_0 x) \right), \quad (4.1)$$

with $\varepsilon_0 = 10^{-3}$. In the middle area of $x \in [-0.18, 0.18]$, since $\varepsilon = \mathcal{O}(1)$, this part is always to be in the kinetic regime. The initial distribution function f is far away from the Maxwellian,

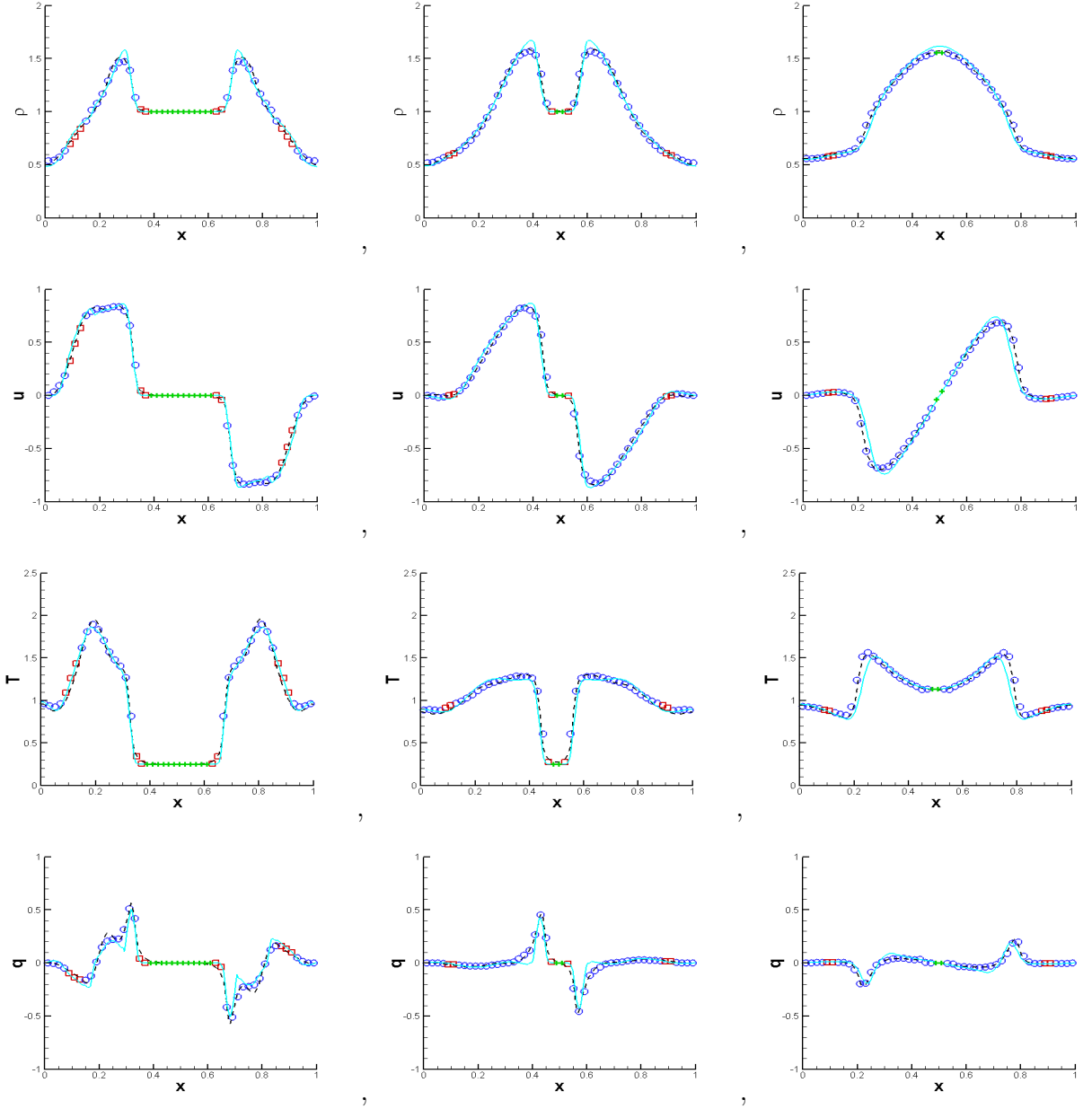


Figure 4.3: Blast wave problem on the domain $[0, 1] \times [-9, 9]$. Symbols: $N_x = 50$ and $N_v = 100$ with NDG3. From left to right: time $t = 0.05, 0.1, 0.25$. From top to bottom, the density ρ , the mean velocity u , the temperature T and the heat flux q . Symbols: ‘+’ is Euler, square is NS, circle is kinetic. Solid line: the NS reference solution. Dashed line: the kinetic reference solution. $\varepsilon = 10^{-2}$, Euler-NS-kinetic.

which is

$$f(x, v, 0) = \frac{\tilde{\rho}}{2(2\pi\tilde{T})^{1/2}} \left[\exp\left(-\frac{|v - \tilde{u}|^2}{2\tilde{T}}\right) + \exp\left(-\frac{|v + \tilde{u}|^2}{2\tilde{T}}\right) \right], \quad (4.2)$$

with

$$\tilde{\rho}(x) = 1 + 0.875 \sin(\omega x), \quad \tilde{T}(x) = 0.5 + 0.4 \sin(\omega x), \quad \tilde{u}(x) = 0.75, \quad (4.3)$$

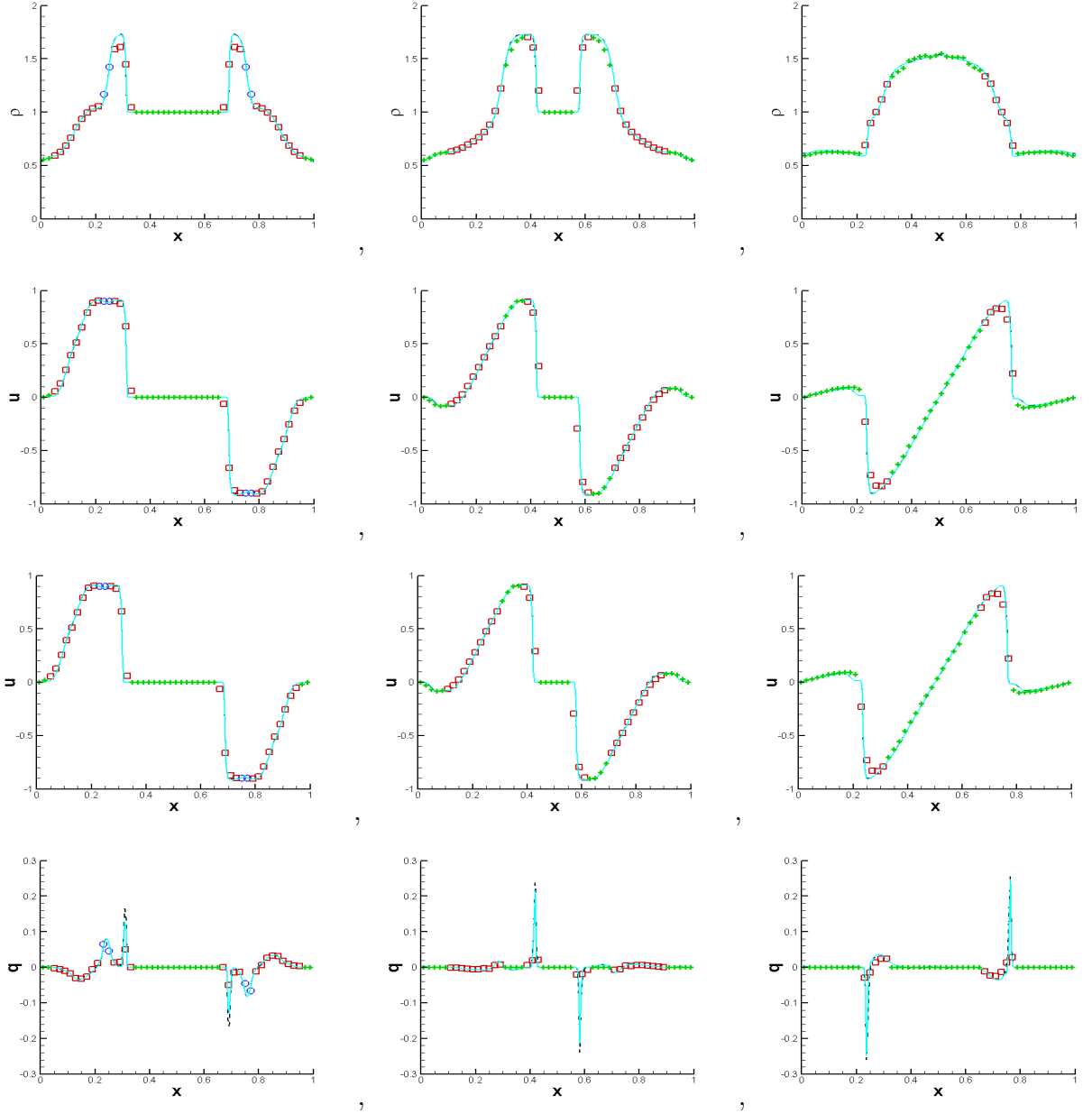


Figure 4.4: Blast wave problem on the domain $[0, 1] \times [-9, 9]$. Symbols: $N_x = 50$ and $N_v = 100$ with NDG3. From left to right: time $t = 0.05, 0.1, 0.25$. From top to bottom, the density ρ , the mean velocity u , the temperature T and the heat flux q . Symbols: ‘+’ is Euler, square is NS, circle is kinetic. Solid line: the NS reference solution. Dashed line: the kinetic reference solution. $\varepsilon = 10^{-3}$, Euler-NS-kinetic.

on the spatial domain $x \in [-L, L]$, where $\omega = \pi/L$ and $L = 0.5$. The initial macroscopic variables are

$$\rho(x, 0) = \tilde{\rho}(x), \quad u(x, 0) = 0, \quad T(x, 0) = \tilde{T}(x) + \tilde{u}(x)^2, \quad (4.4)$$

and the initial Maxwellian distribution is

$$M_U(x, v, 0) = \frac{\rho(x, 0)}{(2\pi T(x, 0))^{1/2}} \exp\left(-\frac{|v - u(x, 0)|^2}{2T(x, 0)}\right). \quad (4.5)$$

Periodic boundary conditions are used for both U and g in the x direction. The velocity domain is taken to be $\Omega_v = [-10, 10]$.

We report the results with 50 cells for the computational solution and 200 cells for the reference solutions in Figures 4.5. Here the NS reference solution is obtained under the time step $\Delta t = \mathcal{O}(h^2)$. However, in the middle region, since $\varepsilon(x) = \mathcal{O}(1)$, the NS solution deviates far away from the kinetic solution and the heat flux oscillates greatly as seen in Figure 4.5. The adaptive algorithm can capture the kinetic solution well. For the computational cost, from Table 4.3, we can observe similar result as the blast wave problem for $\varepsilon = 10^{-3}$. 40% \sim 45% of the computational cost for the Euler-NS-kinetic and NS-kinetic methods, but only 20% for the Euler-kinetic one.

Table 4.3: Comparison of the computational cost (*seconds*) for different indicators. Mixed regime problem.

method	Euler-NS-kinetic	NS-kinetic	Euler-kinetic	Full kinetic
$\varepsilon_0 = 10^{-3}$	362.52	343.44	512.68	631.07

5 Conclusion

We propose a high order hierarchical DG solver for the multi-scale BGK equation. Such hierarchical solver is based on an asymptotic preserving DG IMEX scheme [37], which is formally showed to become a DG scheme for the limiting Euler system and a local DG scheme for the Navier-Stokes system when the Knudsen number is small. Adaptive criteria [23] are applied to automatically switch DG solvers among different regimes (Euler, Navier-Stokes and kinetics), well balancing computational effectiveness and efficiency. Extensive numerical experiments are performed to showcase the proposed scheme in its ability for capturing solution structures and in computational savings.

References

- [1] A. ALAIA AND G. PUPPO, *A hybrid method for hydrodynamic-kinetic flow, Part II: Coupling of hydrodynamic and kinetic models*, Journal of Computational Physics, 232 (2012), pp. 5217 – 5242.
- [2] P. ANDRIES, P. L. TALLEC, J. P. PERLAT, AND B. PERTHAME, *The Gaussian-BGK model of Boltzmann equation with small Prandtl number*, European Journal of Mechanics – B/Fluids, 19 (2000), pp. 813 – 830.

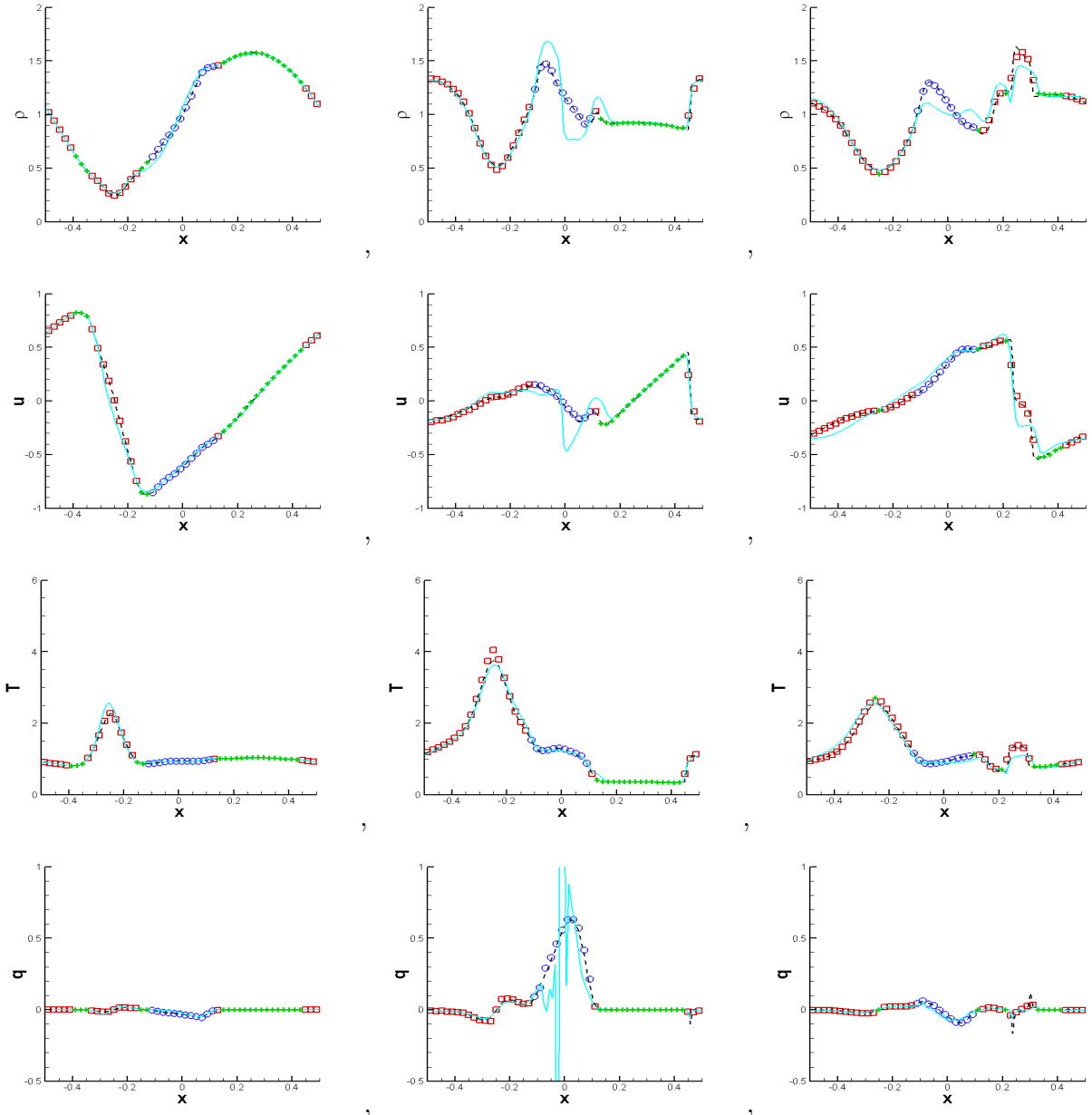


Figure 4.5: Mixed regime problem with $\varepsilon(x)$ with $a_0 = 40$ on the domain $[-0.5, 0.5] \times [-10, 10]$. $N_x = 50$ and $N_v = 100$ with NDG3. Symbols: ‘+’ is Euler, square is NS, circle is kinetic. Solid line: the reference NS solution with $N_x = 100$ and $N_v = 100$. Dashed line: the reference kinetic solution with $N_x = 100$ and $N_v = 100$. From left to right: time $t = 0.1, 0.3, 0.45$. From top to bottom, the density ρ , the mean velocity u , the temperature T and the heat flux q . $\varepsilon_0 = 10^{-3}$, Euler-NS-kinetic.

- [3] U. ASCHER, S. RUUTH, AND R. SPITERI, *Implicit-explicit Runge-Kutta methods for time-dependent partial differential equations*, Applied Numerical Mathematics, 25 (1997), pp. 151–167.
- [4] C. BARDOS, F. GOLSE, AND D. LEVERMORE, *Fluid dynamic limits of kinetic equations*.

- I. Formal derivations*, Journal of Statistical Physics, 63 (1991), pp. 323–344.
- [5] F. BASSI AND S. REBAY, *A high-order accurate discontinuous finite element method for the numerical solution of the compressible Navier–Stokes equations*, Journal of Computational Physics, 131 (1997), pp. 267–279.
 - [6] F. BASSI AND S. REBAY, *Numerical evaluation of two discontinuous Galerkin methods for the compressible Navier–Stokes equations*, International Journal for Numerical Methods in Fluids, 40 (2002), pp. 197–207.
 - [7] C. E. BAUMANN AND J. T. ODEN, *A discontinuous hp finite element method for the Euler and Navier–Stokes equations*, International Journal for Numerical Methods in Fluids, 31 (1999), pp. 79–95.
 - [8] M. BENNOUNE, M. LEMOU, AND L. MIEUSSENS, *Uniformly stable numerical schemes for the Boltzmann equation preserving the compressible Navier–Stokes asymptotics*, Journal of Computational Physics, 227 (2008), pp. 3781–3803.
 - [9] P. L. BHATNAGAR, E. P. GROSS, AND M. KROOK, *A model for collision processes in gases. I. Small amplitude processes in charged and neutral one-component systems*, Physical Review, 94 (1954), pp. 511–525.
 - [10] S. BOSCARINO, L. PARESCHI, AND G. RUSSO, *Implicit-Explicit Runge–Kutta Schemes for Hyperbolic Systems and Kinetic Equations in the Diffusion Limit*, SIAM Journal on Scientific Computing, 35 (2013), pp. A22–A51.
 - [11] S. BOSCARINO AND G. RUSSO, *On a class of uniformly accurate IMEX Runge-Kutta schemes and applications to hyperbolic systems with relaxation*, SIAM Journal on Scientific Computing, 31 (2010), pp. 1926–1945.
 - [12] I. D. BOYD, G. CHEN, AND G. V. CANDLER, *Predicting failure of the continuum fluid equations in transitional hyperbolic flows*, Physical Fluids, 7 (1995), pp. 210 – 219.
 - [13] J. P. BOYD, *Chebyshev and Fourier spectral methods*, Courier Dover Publications, 2001.
 - [14] C. CERCIGNANI, *Mathematical methods in kinetic theory*, Springer, 1969.
 - [15] —, *The Boltzmann equation*, Springer, 1988.
 - [16] —, *Rarefied gas dynamics: from basic concepts to actual calculations*, vol. 21, Cambridge University Press, 2000.
 - [17] B. COCKBURN, S.-Y. LIN, AND C.-W. SHU, *TVB Runge-Kutta local projection discontinuous Galerkin finite element method for conservation laws III: one-dimensional systems*, Journal of Computational Physics, 84 (1989), pp. 90–113.
 - [18] B. COCKBURN AND C.-W. SHU, *The local discontinuous Galerkin method for time-dependent convection-diffusion systems*, SIAM Journal on Numerical Analysis, 35 (1998), pp. 2440–2463.

- [19] P. DEGOND, G. DIMARCO, AND L. MIEUSSENS, *A multiscale kinetic-fluid solver with dynamic localization of kinetic effects*, Journal of Computational Physics, 229 (2010), pp. 4907 – 4933.
- [20] G. DIMARCO, L. MIEUSSENS, AND V. RISPOLI, *An asymptotic preserving automatic domain decomposition for the Vlasov-Poisson-BGK system with applications to plasmas*, Journal of Computational Physics, 274 (2014), pp. 122 – 139.
- [21] F. FILBET AND S. JIN, *A class of asymptotic-preserving schemes for kinetic equations and related problems with stiff sources*, Journal of Computational Physics, 229 (2010), pp. 7625–7648.
- [22] —, *An asymptotic preserving scheme for the ES-BGK model of the Boltzmann equation*, Journal of Scientific Computing, 46 (2011), pp. 204–224.
- [23] F. FILBET AND T. REY, *A hierarchy of hybrid numerical methods for multiscale kinetic equations*, SIAM Journal on Scientific Computing, 37 (2015), pp. A1218 – A1247.
- [24] J. S. HESTHAVEN AND T. WARBURTON, *Nodal discontinuous Galerkin methods: algorithms, analysis, and applications*, vol. 54, Springer-Verlag New York, 2008.
- [25] S. JIN, *Asymptotic preserving (AP) schemes for multiscale kinetic and hyperbolic equations: a review*, Lecture Notes for Summer School on Methods and Models of Kinetic Theory (M&MKT), Porto Ercole (Grosseto, Italy), (2010).
- [26] V. KOLOBOV, R. ARSLANBEKOV, V. ARISTOV, A. A. FROLOVA, AND S. ZABELOK, *Unified solver for rarefied and continuum flows with adaptive mesh and algorithm refinement*, Journal of Computational Physics, 223 (2007), pp. 589 – 608.
- [27] C. D. LEVERMORE, W. J. MOROKOFF, AND B. T. NADIGA, *Moment realizability and the validity of the Navier-Stokes equations for rarefied gas dynamics*, Physics of Fluids, 10 (1998), pp. 3214 – 3226.
- [28] I. LOMTEV AND G. E. KARNIADAKIS, *A discontinuous Galerkin method for the Navier-Stokes equations*, International Journal for Numerical Methods in Fluids, 29 (1999), pp. 587–603.
- [29] L. MIEUSSENS, *Discrete-velocity models and numerical schemes for the Boltzmann-BGK equation in plane and axisymmetric geometries*, Journal of Computational Physics, 162 (2000), pp. 429–466.
- [30] H. NESSYAHU AND E. TADMOR, *Non-oscillatory central differencing for hyperbolic conservation laws*, Journal of Computational Physics, 87 (1990), pp. 408 – 463.
- [31] S. PIERACCINI AND G. PUPPO, *Implicit-explicit schemes for BGK kinetic equations*, Journal of Scientific Computing, 32 (2007), pp. 1–28.
- [32] —, *Microscopically implicit-macroscopically explicit schemes for the BGK equation*, Journal of Computational Physics, 231 (2012), pp. 299–327.

- [33] C.-W. SHU, *High-order finite difference and finite volume WENO schemes and discontinuous Galerkin methods for CFD*, International Journal of Computational Fluid Dynamics, 17 (2003), pp. 107–118.
- [34] S. TIWARI, *Coupling of the Boltzmann and Euler equations with automatic domain decomposition*, Journal of Computational Physics, 144 (1998), pp. 710 – 726.
- [35] S. TIWARI, A. KLAR, AND S. HARDT, *A particle-particle hybrid method for kinetic and continuum equations*, Journal of Computational Physics, 228 (2009), pp. 7109 – 7124.
- [36] —, *Simulations of micro channel gas flows with domain decomposition technique for kinetic and fluid dynamic equations*, in Domain Decomposition Methods in Science and Engineering XXI, Springer, Cham, Switzerland (2012), pp. 197 – 206.
- [37] T. XIONG, J. JANG, F. LI, AND J.-M. QIU, *High order asymptotic preserving nodal discontinuous Galerkin IMEX schemes for the BGK equation*, Journal of Computational Physics, 284 (2015), pp. 70–94.